Environ Sci Pollut Res (2016) 23:23134–23144
DOI 10.1007/s11356-016-7559-3

RESEARCH ARTICLE

Co-exposure to amorphous silica nanoparticles and benzo[a] pyrene at low level in human bronchial epithelial BEAS-2B cells

Jing Wu [1,2] · Yanfeng Shi [1,2] · Collins Otieno Asweto [1,2] · Lin Feng [1,2] · Xiaozhe Yang [1,2] · Yannan Zhang [1,2] · Hejing Hu [1,2] · Junchao Duan [1,2] · Zhiwei Sun [1,2]

Received: 10 July 2016 / Accepted: 29 August 2016 / Published online: 3 September 2016

Abstract Both ultrafine particles (UFP) and polycyclic aromatic hydrocarbons (PAHs) are widely present in the environment, thus increasing their chances of exposure to human in the daily life. However, the study on the combined toxicity of UFP and PAHs on respiratory system is still limited. In this study, we examined the potential interactive effects of silica nanoparticles (SiNPs) and benzo[a]pyrene (B[a]P) in bronchial epithelial cells (BEAS-2B). Cells were exposed to SiNPs and B[a]P alone or in combination for 24 h. Co-exposure to SiNPs and B[a]P enhanced the malondialdehyde (MDA) contents and reduced superoxide dismutase (SOD) and glutathione peroxidase (GSH-Px) activities significantly, while the reactive oxygen species (ROS) generation had a slight increase in the exposed groups compared to the control but not statistically significant. Cell cycle arrest induced by the co-exposure showed a significant percentage increase in G2/M phase cells and a decrease in G0/G1 phase cells. In addition, there was a significant increase in BEAS-2B cells multinucleation as well as DNA damage. Cellular apoptosis was markedly increased even at the low-level co-exposure. Our results suggest that co-exposure to SiNPs and B[a]P exerts synergistic and additive cytotoxic and genotoxic effects.

Keywords Silica nanoparticle · Benzo[a]pyrene · Co-exposure · Cytotoxicity · Genotoxicity

Responsible editor: Philippe Garrigues

Electronic supplementary material The online version of this article (doi:10.1007/s11356-016-7559-3) contains supplementary material, which is available to authorized users.

✉ Junchao Duan
jcduan@ccmu.edu.cn

✉ Zhiwei Sun
zwsun@ccmu.edu.cn

[1] Department of Toxicology and Sanitary Chemistry, School of Public Health, Capital Medical University, Beijing 100069, People's Republic of China

[2] Beijing Key Laboratory of Environmental Toxicology, Capital Medical University, Beijing 100069, People's Republic of China

Introduction

Atmospheric micro/nanoscale particles and various environmental pollutants are the main factors which can induce air pollution (Brown et al. 2013; Kumar et al. 2010; WHO 2013). Recently, it has been demonstrated that toxicity profiles of nanoparticles are more toxic than those of larger particles, because nanoparticles have some features, like small size, dissolution rate, large surface area to mass ratio, etc. (Albanese et al. 2012; Nemmar et al. 2013). Amorphous silica nanoparticles (SiNPs), which are one of the engineering nanoma terials, have been widely applied in drug delivery, cosmetics, industrial manufacturing, and food industries (Argyo et al. 2013; Chaudhry and Castle 2011; Napierska et al. 2010; Sun et al. 2011). This increases the possibility of exposing nanoparticles to humans during its production or use. In addition, nanoparticles are exposed to human through injection, skin penetration, ingestion, or inhalation (Madl and Pinkerton 2009; Napierska et al. 2010; Nemmar et al. 2013). Previous studies have reported that SiNPs cause cytotoxicity, mitochondrial damage, and multinucleation in vitro (Sun et al. 2011; Wang et al. 2013). In vivo research has shown that SiNPs could penetrate the skin, reach different tissues, and then induce the inflammation and vascular homeostasis disorder (Nemmar et al. 2014, 2016).

Moreover, Matassoni et al. have demonstrated that the [Si] clusters substantially increase in the particle matters (PM 2.5 and PM 1) during in-dust days (Matassoni et al. 2011). SiNPs in the fine particulate and ultrafine particulate matters (ultrafine particles (UFP)) significantly contribute to the dust storm event (Kang et al. 2012; Matassoni et al. 2011).

Benzo[a]pyrene (B[a]P) is a human group 1 carcinogen, confirmed by the International Agency for Research on Cancer (IARC) (IARC 2010; Lindeman et al. 2011). B[a]P is a major component of polycyclic aromatic hydrocarbons (PAHs), which has been widely used in evaluating the carcinogenic risk developed by particulate matter (PM) with PAHs absorbed (Gilli et al. 2007; Li et al. 2012; Lim et al. 2014; Škarek et al. 2007). Researches have indicated that B[a]P can induce other toxic effects in cells, such as oxidative stress, DNA damage, cell malignant transformation, and so on (Arlt et al. 2015; Ba et al. 2015; Lim et al. 2014). It has also been proven that B[a]P plays a vital role in lung carcinogenesis (Bruce 2015). However, studies have shown that the potential carcinogenic effects of PAH mixtures are underestimated because interaction effects between B[a]P and other co-existing compounds in the PM have not been considered (Lim et al. 2014). PM and PAHs are ubiquitous in our environment, especially in air pollution (Duan et al. 2016b; Kelly and Fussell 2012). What is more, PAH is one of organic compounds which could be absorbed onto PM (Škarek et al. 2007). The work of Duan et al. showed that co-exposure to SiNPs and B[a]P synergistically elevated the toxic effects on cardiovascular system (Duan et al. 2016b). Studies have shown that the highest female lung cancer rate of China observed in the Xuanwei county, Yunnan Province (Lin et al. 2015), was attributed to the uppermost Permian (C1) coal burning (Downward et al. 2014; Tian et al. 2008). An epidemiologic study has reported that concentrations of UFP and B[a]P in the indoor environments in Xuanwei were much higher than those in the control area (Large et al. 2009). Previous experiments have demonstrated that the toxicity of PAH and SiNP co-exposure is much higher than their individual exposure (Cocco et al. 2001; Large et al. 2009). Based on the previous observations, it is likely that both nanoparticles and PAH could have a great influence on lung cancer. Unfortunately, scientists have not yet reached a consensus on the combined toxicity mechanism of nanoparticles and PAH.

In this study, we focused on the combined toxicity induced by the low-dosage SiNPs and B[a]P co-exposure. The cytotoxicity, oxidative stress, cell cycle arrest, cell multi nucleation, and DNA damage were detected in SiNP and B[a]P alone and co-exposure. Apoptosis was performed by an imaging flow cytometer. These results provide scientific evidence for the combined toxicity of ambient PM with air pollutants in respiratory disease.

Materials and methods

SiNPs and B[a]P

After the generation of amorphous SiNPs based on the Stöber method (Sun et al. 2011), the SiNPs were processed as mentioned in our earlier studies (Duan et al. 2013; Yu et al. 2015). Stock solution of B[a]P (>99.9 %, Sigma, USA) was dissolved in DMSO (≥99.7 %, Sigma, USA) with a volume, which was stored at 4 °C. A transmission electron microscope (TEM) (JEOL, Japan) was used to measure the particle size and shape of SiNPs, which were analyzed by the ImageJ software (National Institutes of Health, Bethesda, USA). The zeta potential and hydrodynamic sizes of SiNPs were tested in ultrapure water and DMEM medium by the Zetasizer (Malvern Instruments, Britain). SiNPs were ultrasonicated for 5 min before using.

Cell culture and co-exposure to SiNPs and B[a]P

The human lung bronchial epithelial cell line (BEAS-2B) was donated from Nanjing Medical University. The BEAS-2B cells were cultured in DMEM medium (Corning, USA) supplemented with 10 % (*v*/*v*) fetal bovine serum (Gibco, USA) and were maintained in a water-saturated atmosphere containing 5 % CO_2 at 37 °C in an incubator. The cells were treated with SiNPs alone, B[a]P alone, and the combined SiNPs and B[a]P for 24 h. SiNP suspension was dispersed using a sonicator (160 W, 20 kHz, 5 min) before mixing with the culture medium to minimize its aggregation.

Assessment of cytotoxicity

A cell counting kit (CCK-8, Dojindo Laboratories, Kumamoto, Japan) was used to evaluate the effects of SiNPs and B[a]P and their co-exposure on cell viability. As the fluorescence of B[a]P can affect the detection of optical density, phosphate-buffered saline (PBS) was used to wash the cells after the exposure to SiNPs (2.5, 5, 10, and 20 μg/mL) and B[a]P (2.5, 5, 10, and 20 μM) for 24 h. Next, 100 μL high-glucose DMEM medium without serum was added to each well; then, 10 μL of CCK-8 solution was added, and the cells were incubated for 2 h at 37 °C. Optical density of each group was measured by a microplate reader (Themo Multiskan MK3, USA) at 450 nm. Based on results of cell viability, the group without significant difference was chosen as the dosage used in the following toxicity experiments. A commercial lactate dehydrogenase (LDH) kit (Jiancheng Bioeng Inst., China) was applied to test LDH leakage following the manual of the kit instruction strictly. After the co-exposure to SiNPs and B[a]P for 24 h, the supernatants were collected for the LDH measurement and a microplate reader at 450-nm absorbance (Themo Multiskan MK3, USA) was applied to detect them.

Assessment of intracellular ROS

The fluorescent probe 2′,7′-dichlorofluorescein diacetate (DCFH-DA) (Sigma, USA) was used to measure the intracellular reactive oxygen species (ROS) generation. After the co-exposure to SiNPs and B[a]P for 24 h, the cells were washed thrice with PBS and were co-incubated with DCFH-DA at 37 °C for 30 min in the dark. Subsequently, the medium was removed and the cells were harvested. The percentage of positive cells and fluorescent intensities were detected through a flow cytometer (Becton Dickinson, USA).

Oxidative damage assessment

After the co-exposure to SiNPs and B[a]P for 24 h, the cells were washed thrice with ice-cold PBS. And then, the cells were harvested and centrifuged for 10 min at 4 °C and 1000 rpm. The cells were resuspended in ice-cold PBS, and the protein was extracted by using an ultrasonic cell disruptor (JY 92-II, SCIENTZ, China). The concentrations of extracted protein were detected by the bicinchoninic acid (BCA) protein assay (Jiancheng Bioeng Inst., China). Malondialdehyde (MDA), superoxide dismutase (SOD), and glutathione peroxidase (GSH-Px) consisted in the protein were detected by commercially available diagnostic kits (Jiancheng Bioeng Inst., China). All indexes were measured following the manual of the kit strictly.

Cell cycle assessment

The BEAS-2B cells were seeded into a six-well plate. Different concentrations of SiNPs and B[a]P were added. After 24 h of incubation, the cells were harvested and centrifuged under the condition of 1200 rpm for 5 min at 4 °C. Then, the cells were washed thrice with cold PBS, fixed in cold 70 % ethanol, and frozen at 4 °C overnight. The cells were centrifuged at 1500 rpm for 10 min at 4 °C and were washed thrice with ice-cold PBS in the following day. Subsequently, the liquid was removed and 100 μL of RNase was added in each sample, which was incubated for 30 min at 37 °C. Then, 400 μL propidium iodide (PI) was added in each sample, which was incubated for 30 min at 4 °C in the dark. The flow cytometer (Becton Dickinson, USA) was used to examine the DNA content.

Multinucleation observation

After the co-exposure to SiNPs and B[a]P for 24 h, the liquid was removed and PBS was used to wash the cells three times. According to the manual of Wright-Giemsa Assay Reagent Kit (KeyGen Biotech, China), the cells were observed in Giemsa staining. Morphology investigations were observed by the inverted phase contrast microscope (Olympus, Japan). Fields were selected randomly, and the numbers of binucleated and multinucleated cells were counted to calculate the rate of total multinucleated cells.

DNA damage assay

After the co-exposure to SiNPs and B[a]P for 24 h, a single-cell gel electrophoresis (SCGE) kit (Biolab, China) was used to measure DNA damage. PBS was used to resuspend the cells. Ten-microliter cell suspensions and 90 μL agarose were mixed and dropped to agarose-coated slides. Coverslips were used to cover the agarose-coated slides, which were then frozen at 4 °C for 4 min. The slides were immersed in fresh lysis solution for 1.5 h at 4 °C in the dark after the removal of the coverslips. And then, the slides were subjected to electrophoresis under the conditions 25 V, 300 mA, and 1 V/cm for 30 min for DNA unwinding. After the electrophoresis, the slides were dried in the air. The PI was used to stain the slides, which is detected by a fluorescence microscope (Olympus, Japan). Then, the CASP software was adopted to compute the indexes of DNA damage.

Apoptosis analysis

The BEAS-2B cells in the logarithmic phase were seeded into a six-well plate. After the co-exposure to SiNPs and B[a]P for 24 h, the ice-cold PBS was used to wash the cells three times, which were collected for centrifugation at 2000 rpm for 5 min and resuspended with 500 μL binding buffer. Then, 5 μL fluorescein isothiocyanate-conjugated Annexin V antibody (Annexin V/FITC) and 5 μL PI (KeyGen Biotech, China) were added. The mixture was incubated for 15 min at room temperature without light. A total of 10,000 cells were analyzed by an Amnis ImageStream multispectral imaging flow cytometer system (Amnis, USA). The samples were collected under the environment of low speed, and approximately 5000 events were gated and recorded. The data was analyzed using IDEAS 6.0 (Amnis, USA) and FlowJo 7.6 (Tree Star, USA).

Statistical analysis

The SPSS 17.0 software (SPSS Inc., USA) was used to perform all the statistical analyses. Statistical analysis was carried out through one-way analysis of variance (ANOVA), while $p < 0.05$ is statistically significant. According to the statistical method described in our previous study (Yu et al. 2015), the factorial design experiments and two-factorial ANOVA were used to evaluate the combined SiNPs and B[a]P interactions. Multinucleated cell numbers and rate were analyzed through the chi-square test and regarded as frequencies. Others were regarded as mean ± standard deviation (SD).

Results

Characterization of SiNPs

As shown in Fig. 1, the amorphous SiNPs were near-spherical and evenly distributed, which were observed by transmission electron microscopy. Five hundred particles were analyzed by ImageJ software to determine the particle size distribution. The average size and the purity of SiNPs were 49.56 ± 5.17 nm and above 99.9 %, respectively. The hydrodynamic diameter and zeta potential of SiNPs were measured in ultrapure water and DMEM exposure media. As shown in Table 1 and Supplementary Table S1, a fairly stable suspension in both ultrapure water and DMEM medium was observed.

Cytotoxic effect of SiNPs and B[a]P

To investigate the cytotoxicity of co-exposure to the SiNPs and B[a]P on the BEAS-2B cells, cell viability and LDH activity were measured. CCK-8 kit was used to estimate cell viability. Figure 2 demonstrates that cell viability was moderately reduced in a dose-dependent manner by SiNPs and B[a]P. B[a]P and SiNPs (Supplementary Fig. S1) did not have a significant difference on cell viability compared to the control at 5 μM and 5 μg/mL concentrations, respectively. However, both SiNPs and B[a]P decreased the cell viability to 96.58 ± 1.25 and 92.62 ± 3.74 % of the control, respectively (Fig. 2a, b). In order to further investigate the interactive effect between SiNPs and B[a]P, the 5 μg/mL of SiNPs and 5 μM of B[a]P were chosen. As shown in Fig. 2c, a synergistic reduction of cell viability was observed after the co-exposure to SiNPs and B[a]P for 24 h. The cell viabilities in SiNPs, B[a]P, and the co-exposed group were 95.92, 93.33, and 89.06 %, respectively (Fig. 2c). At the same time, LDH activity increased significantly in the co-exposed group compared to the control (Fig. 2d). These results indicate additive interaction on cell viability of the co-exposure of SiNPs and B[a]P and synergistic interaction on their LDH activity (Supplementary Figs. S2 and S3), thus enhancing the cytotoxicity of individual SiNPs or B[a]P.

Intracellular ROS

ROS generation is an indicator of oxidative stress, which is mainly affected by nanoparticle exposure. The intracellular ROS level of the BEAS-2B cells exposed to SiNPs and B[a]P for 24 h was determined by flow cytometry. Although the generation of ROS in all the treatment groups had no statistical significance, the level of ROS generation was increased slightly (1.18-fold of the control) after co-exposure to SiNPs and B[a]P (Fig. 3a). This suggests that the intracellular ROS of the BEAS-2B cells is not the dominant response in oxidative stress at the low-level co-exposure.

Oxidative damage

After the co-exposure to SiNPs and B[a]P for 24 h, the content of MDA and the activity of SOD and GSH-Px were detected. The result demonstrated that MDA was increased remarkably (Fig. 3b), while the SOD and GSH-Px activities were declined significantly in the BEAS-2B cells after alone exposure and co-exposure to SiNPs and B[a]P (Fig. 3c, d). Moreover, compared with the control, the co-exposed group had high MDA levels and lower SOD and GSH-Px activities significantly. In other words, these results indicate that SiNPs and B[a]P synergistically disturbed the redox balance in the BEAS-2B cells (Supplementary Figs. S4, S5, and S6).

Cell cycle arrest

In order to analyze the potential mechanisms of cell growth inhibition, the BEAS-2B cells were co-exposed to SiNPs and B[a]P for 24 h. Arrest of cell cycle was examined by flow cytometry. The percentages of G0/G1 phase had decreased markedly in the BEAS-2B cells (Fig. 4a and Supplementary Fig. S7), while the number of G2/M phase cells increased

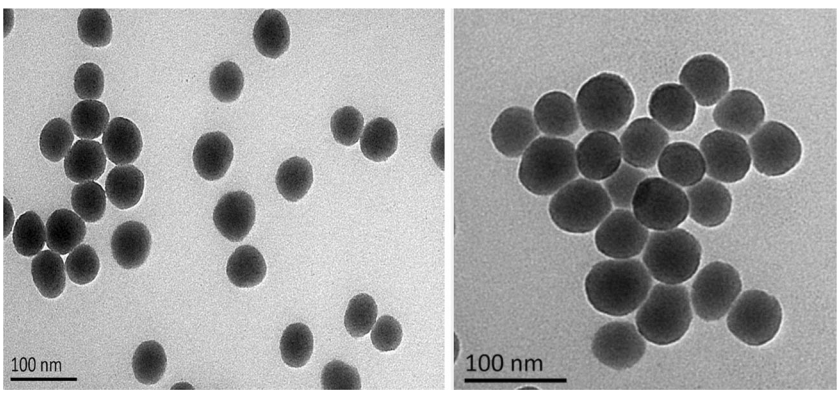

Fig. 1 Transmission electron microscopic image of 49.56 nm amorphous silica nanoparticles

Table 1 The hydrodynamic diameter and zeta potential of SiNPs in different dispersion media

Medium	Hydrodynamic sizes (nm)	Zeta potential (mV)
Ultrapure water	79.44 ± 0.33	−64.05 ± 0.78
DMEM medium	72.10 ± 0.80	−33.25 ± 1.41

significantly regarding the co-exposed cells (Fig. 4b and Supplementary Fig. S8). In summary, SiNPs and B[a]P arrest the cell cycle in the G2/M phase; thus, G2 or M phase was arrested in BEAS-2B cells.

Cell multinucleation

Figure 5 demonstrates the results of a representative multinucleation experiment in which BEAS-2B cells were co-exposed to SiNPs and B[a]P for 24 h. Morphology investigation with Giemsa was observed by the inverted phase contrast microscope. The nuclei were stained in blue-purple, while the cytoplasm in pink. The morphology indicated that most of the nuclei in the control were normal round and homogeneously stained. The numbers of binucleated cells and multinucleated cells in the co-exposed group increased significantly (5.86-fold of the control) in the BEAS-2B cells (Table 2).

Effects on DNA damage of SiNPs and B[a]P

After the co-exposure to SiNPs and B[a]P for 24 h, the DNA damage was measured through a comet assay. The magnification was reported by a ×200 fluorescence microscope. DNA damage was reflected more severely in the co-exposed group, as shown in Fig. 6. The index value in the co-exposure group was significantly higher than that in the control (Fig. 6 and Supplementary Fig. S9). It is suggested that co-exposure to SiNPs and B[a]P can result in additive interaction on the DNA damage.

Induction of apoptosis in BEAS-2B cells

As shown in Figs. 7 and 8, the BEAS-2B cells were detected by using the imaging flow cytometer after the cells were treated with the SiNPs and B[a]P alone or co-exposed for 24 h. The apoptotic rates in the co-exposed groups were significantly increased than those in the single groups and the control (Fig. 7). Obviously, morphological changes in the BEAS-2B cells were observed after the co-exposure to SiNPs and B[a]P (Fig. 8). Intact and evenly stained nuclei were demonstrated in the control, while membranolysis, phosphatidylserine eversion from the membrane, and cell membrane indicating green and red fluorescence were found in the co-exposure group (Fig. 8). It demonstrated that co-exposure to SiNPs and B[a]P significantly enhanced the apoptotic rate compared with

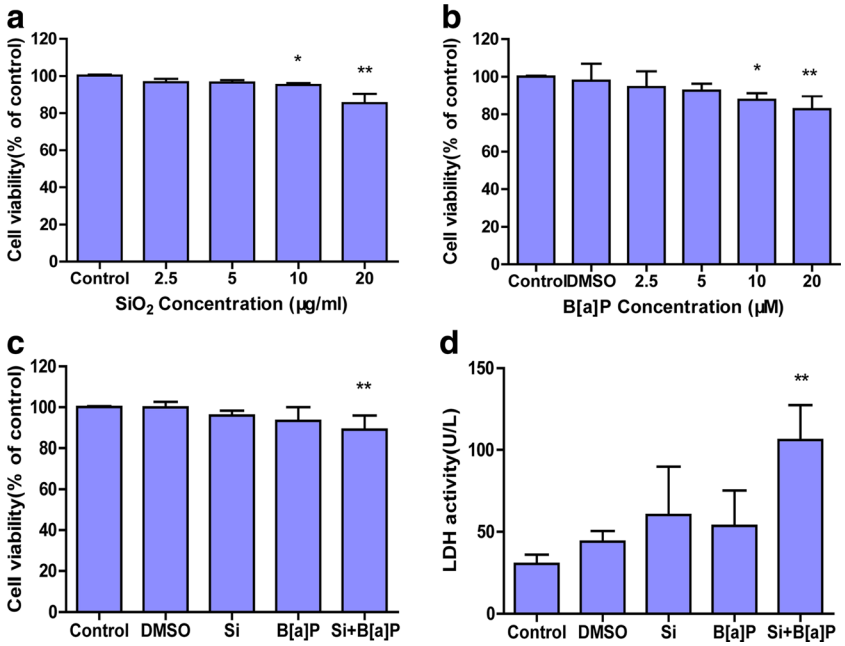

Fig. 2 Cytotoxicity of BEAS-2B cells induced by SiNPs and B[a]P. **a** Cell viability of SiO_2 at different concentrations. **b** Cell viability of B[a]P at different concentrations. **c** Cell viability of BEAS-2B cells exposed to SiO_2 (5 μg/mL), B[a]P (5 μM), and their mixture (5 μg/mL + 5 μM) for 24 h. **d** LDH activity of BEAS-2B cells after being exposed to SiO_2 (5 μg/mL), B[a]P (5 μM), and their mixture (5 μg/mL + 5 μM) for 24 h. Data are expressed as means ± SD from three independent experiments. $^*p < 0.05$, $^{**}p < 0.01$ compared with untreated control

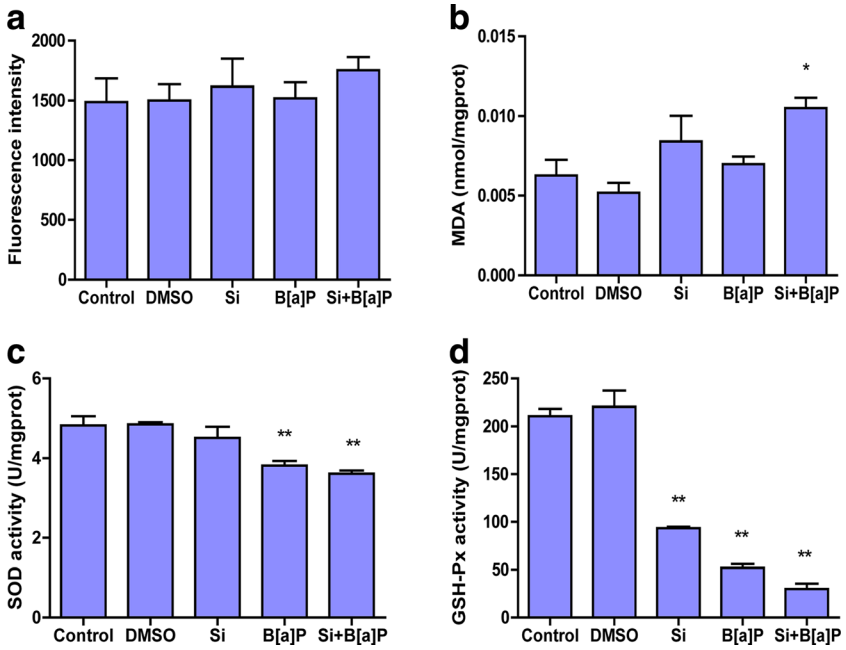

Fig. 3 Oxidative stress and oxidative damage in BEAS-2B cells after co-exposure to SiNPs (5 μg/mL) and B[a]P (5 μM) for 24 h. **a** ROS level. **b** MDA contents of lipid peroxidation. **c** SOD activity reduction. **d** GSH-Px activity reduction. Data are expressed as means ± SD from three independent experiments. *$p < 0.05$, **$p < 0.01$ compared with untreated control

the control in the BEAS-2B cells (Fig. 7 and Supplementary Fig. S10).

Discussion

Great attention has been devoted to the adverse health effects, such as cardiovascular and pulmonary diseases induced by combined toxicity of the PM compositions (Atkinson et al. 2010; Breitner et al. 2011; Franck et al. 2011). Nanoparticles, which are the major components of PM, can absorb environmental pollutants, including large amounts of organic contaminants such as confirmed human carcinogen B[a]P and inorganic harmful metals (Huang et al. 2016; Kumar et al. 2010). However, the studies focusing on the combined toxicity of nanoparticles and B[a]P on human respiratory system are still not clear, and the mechanisms involved in the combined effects are still not well understood. Therefore, we investigated the combined toxicity effects of low-level SiNPs and B[a]P co-exposure to respiratory system using BEAS-2B cells. In our study, the cells were treated with SiNPs alone, B[a]P alone, and the combined SiNPs and B[a]P. The concentration of SiNPs and B[a]P, which did not have a significant difference compared to the control in cell viability, respectively, was chosen. What is more, the concentration of B[a]P in the present study is a general dose used in the in vivo and in vitro experiments in toxicology studies (Chen et al. 2013; McClean et al. 2004, Melchini et al. 2011; Vakharia et al. 2001; Zhu et al. 2014). The experiment indicated that the toxicity induced by the co-exposure to SiNPs and B[a]P was higher than that induced by the individual compounds in the BEAS-2B cells.

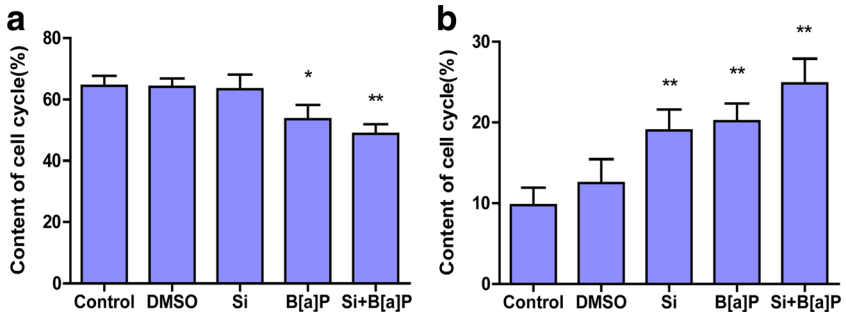

Fig. 4 G2/M phase cell cycle arrest of BEAS-2B cells after co-exposure to SiNPs (5 μg/mL) and B[a]P (5 μM) for 24 h. The BEAS-2B cell cycle was measured by flow cytometry. **a** The percentage of cells in G0/G1 phase decreased, and **b** the percentage of cells in G2/M phase increased significantly. Data are expressed as means ± SD from three independent experiments. *$p < 0.05$, **$p < 0.01$ compared with untreated control

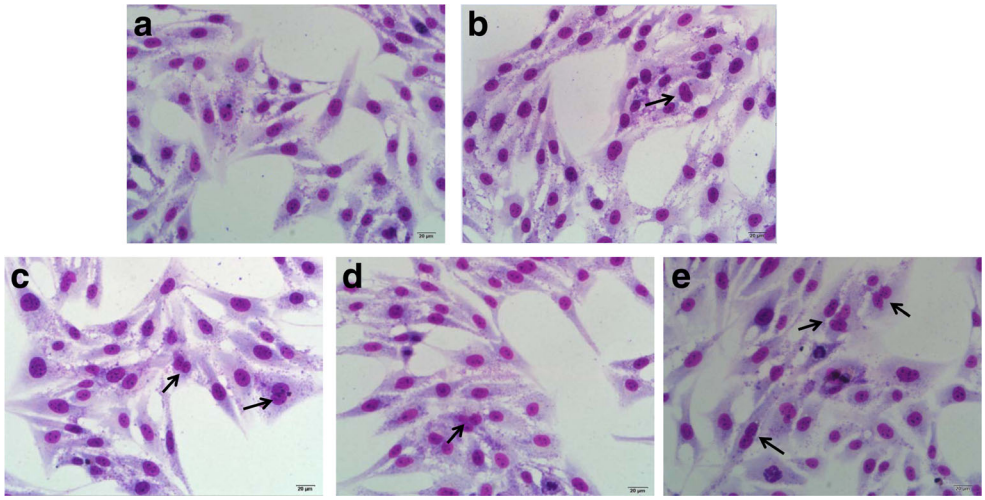

Fig. 5 Multinucleation in BEAS-2B cells after co-exposure to SiNPs (5 μg/mL) and B[a]P (5 μM) for 24 h. **a** Control group. **b** DMSO group. **c** SiO_2 group. **d** B[a]P group. **e** Si + B[a]P group. The cell nucleus and cytoplasm were stained by Giemsa. Binucleated cells and multinucleated cells were observed by an inverted phase contrast microscope

In addition, our previous study demonstrated that SiNPs and B[a]P mixtures have a high absorption and favorable thermal stability at low exposure levels (Duan et al. 2016b). The cytotoxicity of co-exposure was significantly enhanced in the BEAS-2B cells after the co-exposure to SiNPs and B[a]P for 24 h (Fig. 2). The lowest cell viability (Fig. 2c) and highest LDH activity (Fig. 2d) were observed for co-exposure. The synergistically enhanced cytotoxic effect observed by our experiment is similar to the previous reports on SiNPs and B[a]P in zebrafish embryos (Duan et al. 2016b). In addition, our previous research analyzed the internalization and intracellular distribution of SiNPs by TEM image in BEAS-2B cells and suggested that the cellular uptake of SiNPs was related to the adverse effects in cells such as mitochondrial damage and autophagy (Li et al. 2016). We showed that the SiNPs could uptake in the HepG2 (human hepatoma cell line) cells through the endocytosis, disperse in cytoplasm, and deposit into some organelles, such as mitochondria, lysosomes, and so on (Sun et al. 2011). We also found that the SiNPs were internalized into human umbilical vein endothelial cell line (HUVEC) cells, disturbed the cytoskeleton in a dose-dependent manner, and induced mitochondrial damage and autophagic vacuoles accumulation in the HUVECs (Duan et al. 2014). In summary, the SiNPs could enter the cells such as BEAS-2B cells through different pathways, localize in cytoplasm as well as organelles, and induce cytotoxic effects and genotoxicity.

Oxidative stress and inflammation have been proposed as the major mechanisms responsible for the toxicity induced by nanoparticles in vivo or in vitro (Alinovi et al. 2015; Duan et al. 2013; Khatri et al. 2013; Mendoza et al. 2014). To evaluate the potential mechanisms of co-exposure, the oxidative stress and damage indexes including ROS, MDA, SOD, and GSH-Px were determined. Our study demonstrated that the cellular oxidative stress and damage were enhanced. This phenomenon can lead to the imbalance of redox state after the co-exposure. In vivo, the role

Table 2 Number of binucleated and multinucleated cells induced by SiNPs and B[a]P

Group	Cell count	Binucleated and multinucleated cells(n)	Rate of binucleated and multinucleated cells (%)
Control	500	7	1.4
DMSO	500	8	2
SiO_2	500	28	5.6*
B[a]P	500	21	4.2*
Si + B[a]P	500	41	8.2*

*$p < 0.05$ compared with control group using chi-square test

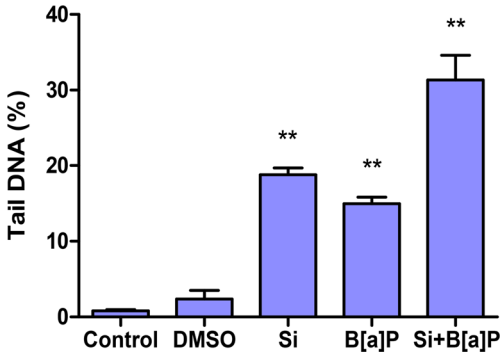

Fig. 6 The tail DNA% of BEAS-2B cells after co-exposure to SiNPs (5 μg/mL) and B[a]P (5 μM) for 24 h evaluated by using a comet assay. Data are expressed as means ± SD from three independent experiments. *$p < 0.05$, **$p < 0.01$ compared with untreated control

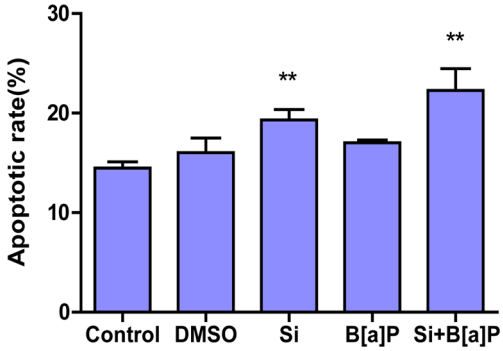

Fig. 7 Apoptosis of BEAS-2B cells after co-exposure to SiNPs (5 μg/mL) and B[a]P (5 μM) for 24 h. Annexin V-FITC/PI assay was applied to measure the apoptotic rate. Data are expressed as means ± SD from three independent experiments. *$p < 0.05$, **$p < 0.01$ compared with untreated control

of free radicals is to produce peroxidation; the end product of lipid oxidation is MDA. SOD, one of the enzymatic antioxidants, is responsible for scavenging free radicals in the body, maintaining the steady status of hydrogen peroxide (Jomova and Valko 2011). It is usually measured together with another anti-oxidative enzyme GSH-Px. Protecting the organism from oxidative damage and reducing free hydrogen are the main biological roles of GSH-Px. In this study, the increase of MDA content and the rapid decrease of SOD and GSH-Px activity were observed after the co-exposure to SiNPs and B[a]P (Fig. 3). This indicates that SOD and GSH-Px play a vital role in combating the hazardous effects of SiNPs and B[a]P-induced free radicals. However, compared with the control, ROS generation of all co-exposed groups did not have statistical significance (Fig. 3a). This phenomenon is similar to our previous study, which suggested that the predominant response was not the production of ROS but the inflammation in the co-exposure to SiNPs and B[a]P at the low dosage (Duan et al. 2016b). Pink et al. found that ROS generation is the same after the co-exposure to B[a]P and carbon black particles on the human endothelial cell line EA.hy 926 (Pink et al. 2014). In other words, the co-exposure to SiNPs and B[a]P produced MDA, reduced SOD and GSH-Px activities, enhanced the effects on BEAS-2B cells, and led to redox imbalance, which is an initial step of carcinogenesis. Another possible explanation is that the dosage of co-exposure was too low to generate ROS in detectable levels (Pink et al. 2014). The potential mechanisms should be explored in the future work.

Cell cycle is a series of events resulting in cell division and replication (Cai et al. 2015). Some conditions, such as nutrient depletion, DNA damage, and growth factor withdrawal, which are not suitable for DNA replication, can restrict the cell cycle progression (Jones et al. 2005; Shi et al. 2010). In our study, a significant increase was found in the percentage of the co-exposed cell group arrested in G2/M phase (Fig. 5b). In addition, the percentage of multinucleation in BEAS-2B cells was increased due to cell cycle alterations (Fig. 6). Based on the phenomenon that L-02 cells arrested in G2/M phase of the cell cycle after the cells are treated with SiNPs, a previous study proposed an assumption that these cells were arrested in M

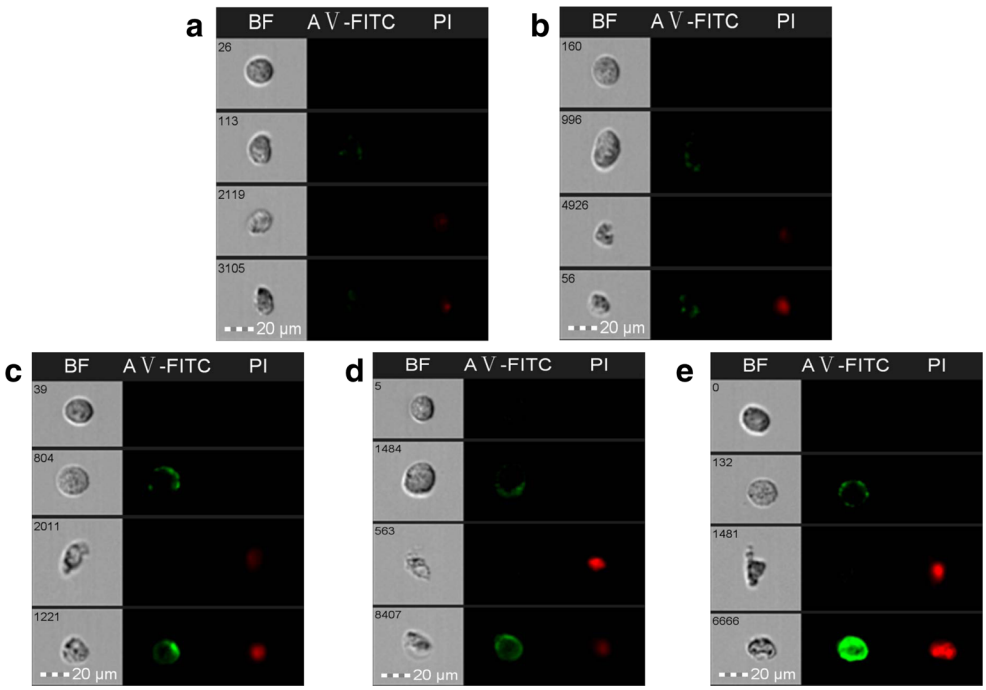

Fig. 8 Apoptosis of BEAS-2B cells after co-exposure to SiNPs (5 μg/mL) and B[a]P (5 μM) for 24 h. The representative images of BEAS-2B apoptosis were measured by a imaging flow cytometer. **a** Control group. **b** DMSO group. **c** Single SiO_2-treated group. **d** Single B[a]P-treated group. **e** Co-treatment group

phase rather than in G2 phase (Wang et al. 2013). Zhu et al. found that the exposure to B[a]P in the BEAS-2B cells induced cell cycle arrested at G2/M phase (Zhu et al. 2014). In the processing of mitosis, the cytokinesis and replicated chromosomes should be precisely distributed in space and time (He et al. 2000; Wang et al. 2013). Chromosomes that separated unsuccessfully into each daughter cell can induce polyploidy or aneuploidy (Leverson et al. 2002), which plays a vital role in lung tumorigenesis and progression (Balsara and Testa 2002; Pailler et al. 2015).

It is usual that the cell cycle alteration is linked to DNA damage (Hamouchene et al. 2011; Puente et al. 2014). DNA damage response can activate the G2/M transition checkpoint, which is a non-genomic and rapid response system (Rieder 2011). Recent studies have been demonstrated that oxidative stress and/or inflammation could lead to particulate-mediated DNA oxidation damage (Møller et al. 2014; Nemmar et al. 2016). SiNPs induced DNA damage by entering the cells mainly through actin-mediated endocytosis, such as the macropi nocytosis pathway (Nabeshi et al. 2011). The results of an in vivo study indicated that pulmonary inflammation modulated the bioactivation of B[a]P and enhanced formation of covalent B[a]P-DNA adducts, which can induce the respiratory tract DNA damage subsequently (Arlt et al. 2015). Furthermore, our previously study demonstrated that the SiNPs contained numerous hydroxyl radical (·OH) on surface, which induced adverse toxic effect in cells (Duan et al. 2016a). The surface area of nanoparticles is much higher than that of larger particles, which could enhance the probability to absorb some organic compounds such as PAHs and lead to larger health risks to humans (Donaldson et al. 2005; EPA 2002). It is well known that co-exposure to SiNPs and B[a]P can induce a higher toxic effect in the cells than the individual chemical exposure.

In an in vitro study, B[a]P could induce the expression levels of CYP1A1 and CYP1B1 and intensify p53 activation and PARP-1 protein expression (Zhu et al. 2014). Our previous study has reported that SiNPs co-exposed with other known carcinogens (such as B[a]P and MeHg) could induce DNA damage and inhibit DNA repair (Yu et al. 2015). However, whether the synergistic cytotoxicity of SiNPs and B[a]P resulted to DNA and chromosomal damage is difficult to detect. The interactive effects of SiNPs and B[a]P on the genotoxicity were evaluated further through the comet assay and apoptotic assay. DNA damage was increased markedly in BEAS-2B cells after the co-exposure (Fig. 6). DNA damage induced by SiNPs and B[a]P could not be repaired efficiently. The result suggested that co-exposure to SiNPs and B[a]P could enhance DNA damage, which might promote tumorigenesis. As a unique type of programmed cell death, apoptosis plays an important role in the maintenance of homeostasis and elimination of damaged cells (Ouyang et al. 2012). Dysregulation of processes controlling apoptosis often contributes to the development of neoplasia (Ouyang et al. 2012). An earlier study had found that nearly half of the cells which progressed to mitosis unsuccessfully are bound to apoptosis after the exposure to SiNPs (Wang et al. 2013). In our study, imaging flow cytometry was chosen to measure the apoptotic rate because its fluorescence sensitivity and cell resolution are better than those of the ordinary flow cytometry. What is more, the imaging flow cytometry can not only analyze cell groups but also provide morphological images of individual cells. According to the analysis of the imaging flow cytometry, the highest apoptosis rate was observed in cells co-exposed to SiNPs and B[a]P (Fig. 7). The damage of the cell membrane and "the little tail" of the cell were observed, especially in the co-exposed group (Fig. 8). It is assumed that an increase of the apoptotic rate after the co-exposure is a reflection of elevated DNA damage or removal of abnormal cells in the BEAS-2B cells. In an in vitro study, it was demonstrated that the number of apoptotic cells significantly increased after the B[a]P exposure in the oral mucosa cells (Wannhoff et al. 2013), and our previous study found that SiNPs inhibited cell growth, induced apoptosis in exposed cells, and induced the toxicity of endothelial cells via Chk1-dependent G2/M signaling pathway (Duan et al. 2013, Wang et al. 2013), which are consistent with the present findings.

Conclusion

In summary, the SiNPs and B[a]P co-exposure caused oxidative damage, cell multinucleation, cell cycle arrest, DNA damage, and apoptosis in BEAS-2B cells. Oxidative damage can be represented as a significant increase in MDA and a reduction in SOD and GSH-Px activities after the co-exposure. The imbalance of redox state and arrest of cell cycle led to the DNA damage and cellular apoptosis through the combination effects of SiNPs and B[a]P even at the low-level co-exposure. In subsequent studies, there is a need to focus on pathways and molecular mechanisms of combined toxicity in both in vitro and in vivo experiments in order to provide more insights into mechanisms involved in combined toxicity.

Acknowledgments This work was supported by the National Natural Science Foundation of China (Nos. 81230065 and 81571130090) and Special Project of Beijing Municipal Science & Technology Commission (KZ201410025022).

Compliance with ethical standards

Conflict of interest The authors declare they have no conflict of interest.

References

Albanese A, Tang PS, Chan WC (2012) The effect of nanoparticle size, shape, and surface chemistry on biological systems. Annu Rev Biomed Eng 14:1–16

Alinovi R, Goldoni M, Pinelli S, Campanini M, Aliatis I, Bersani D, Lottici PP, Iavicoli S, Petyx M, Mozzoni P (2015) Oxidative and pro-inflammatory effects of cobalt and titanium oxide nanoparticles on aortic and venous endothelial cells. Toxicol in Vitro 29:426–437

Argyo C, Weiss V, Bräuchle C, Bein T (2013) Multifunctional mesoporous silica nanoparticles as a universal platform for drug delivery. Chem Mater 26:435–451

Arlt VM, Krais AM, Godschalk RW, Riffo-Vasquez Y, Mrizova I, Roufosse CA, Corbin C, Shi Q, Frei E, Stiborova M (2015) Pulmonary inflammation impacts on CYP1A1-mediated respiratory tract DNA damage induced by the carcinogenic air pollutant benzo [a] pyrene. Toxicol Sci 146:213–225

Atkinson RW, Fuller GW, Anderson HR, Harrison RM, Armstrong B (2010) Urban ambient particle metrics and health: a time-series analysis. Epidemiology 21:501–511

Ba Q, Li J, Huang C, Qiu H, Li J, Chu R, Zhang W, Xie D, Wu Y, Wang H (2015) Effects of benzo [a] pyrene exposure on human hepatocellular carcinoma cell angiogenesis, metastasis, and NF-κB signaling. Environ Health Perspect 123:246

Balsara BR, Testa JR (2002) Chromosomal imbalances in human lung cancer. Oncogene 21:6877–6883

Breitner S, Liu L, Cyrys J, Brüske I, Franck U, Schlink U, Leitte AM, Herbarth O, Wiedensohler A, Wehner B (2011) Sub-micrometer particulate air pollution and cardiovascular mortality in Beijing, China. Sci Total Environ 409:5196–5204

Brown JS, Gordon T, Price O, Asgharian B (2013) Thoracic and respirable particle definitions for human health risk assessment. Part Fibre Toxicol 10:1

Bruce V (2015) Effects of low-dose gamma radiation in a murine model of benzo [a] pyrene-induced lung cancer.

Cai X, Hu X, Tan X, Cheng W, Wang Q, Chen X, Guan Y, Chen C, Jing X (2015) Metformin induced AMPK activation, G0/G1 phase cell cycle arrest and the inhibition of growth of esophageal squamous cell carcinomas in vitro and in vivo. PLoS One 10:e0133349

Chaudhry Q, Castle L (2011) Food applications of nanotechnologies: an overview of opportunities and challenges for developing countries. Trends Food Sci Technol 22:595–603

Chen Y, Huang C, Bai C, Gao H, Ma R, Liu X, Dong Q (2013) Benzo [α] pyrene repressed DNA mismatch repair in human breast cancer cells. Toxicology 304:167–172

Cocco P, Rice CH, Chen JQ, McCawley MA, McLaughlin JK, Dosemeci M (2001) Lung cancer risk, silica exposure, and silicosis in Chinese mines and pottery factories: the modifying role of other workplace lung carcinogens. Am J Ind Med 40:674–682

Donaldson K, Tran L, Jimenez LA, Duffin R, Newby DE, Mills N, MacNee W, Stone V (2005) Combustion-derived nanoparticles: a review of their toxicology following inhalation exposure. Part Fibre Toxicol 2:1

Downward GS, Hu W, Large D, Veld H, Xu J, Reiss B, Wu G, Wei F, Chapman RS, Rothman N (2014) Heterogeneity in coal composition and implications for lung cancer risk in Xuanwei and Fuyuan counties, China. Environ Int 68:94–104

Duan J, Hu H, Li Q, Jiang L, Zou Y, Wang Y, Sun Z (2016a) Combined toxicity of silica nanoparticles and methylmercury on cardiovascular system in zebrafish (*Danio rerio*) embryos. Environ Toxicol Pharmacol 44:120–127

Duan J, Yu Y, Li Y, Wang Y, Sun Z (2016b) Inflammatory response and blood hypercoagulable state induced by low level co-exposure with silica nanoparticles and benzo [a] pyrene in zebrafish (*Danio rerio*) embryos. Chemosphere 151:152–162

Duan J, Yu Y, Li Y, Yu Y, Li Y, Zhou X, Huang P, Sun Z (2013) Toxic effect of silica nanoparticles on endothelial cells through DNA damage response via Chk1-dependent G2/M checkpoint. PLoS One 8: e62087

Duan J, Yu Y, Yu Y, Li Y, Huang P, Zhou X, Peng S, Sun Z (2014) Silica nanoparticles enhance autophagic activity, disturb endothelial cell homeostasis and impair angiogenesis. Part Fibre Toxicol 11:1–13

EPA (2002) Health assessment document for diesel engine exhaust. National Center for Environmental Assessment

Franck U, Odeh S, Wiedensohler A, Wehner B, Herbarth O (2011) The effect of particle size on cardiovascular disorders—the smaller the worse. Sci Total Environ 409:4217–4221

Gilli G, Pignata C, Schilirò T, Bono R, La Rosa A, Traversi D (2007) The mutagenic hazards of environmental PM2.5 in Turin. Environ Res 103:168–175

Hamouchene H, Arlt VM, Giddings I, Phillips DH (2011) Influence of cell cycle on responses of MCF-7 cells to benzo [a] pyrene. BMC Genomics 12:1

He X, Asthana S, Sorger PK (2000) Transient sister chromatid separation and elastic deformation of chromosomes during mitosis in budding yeast. Cell 101:763–775

Huang Y, Fulton AN, Keller AA (2016) Optimization of porous structure of superparamagnetic nanoparticle adsorbents for higher and faster removal of emerging organic contaminants and PAHs. Environ Sci Water Res Technol 2:521–528

IARC (2010) Some non-heterocyclic polycyclic aromatic hydrocarbons and some related exposures. IARC Monog Eval Carcinog Risks Humans/World Health Org, Int Agency Res Cancer 92:1

Jomova K, Valko M (2011) Advances in metal-induced oxidative stress and human disease. Toxicology 283:65–87

Jones RG, Plas DR, Kubek S, Buzzai M, Mu J, Xu Y, Birnbaum MJ, Thompson CB (2005) AMP-activated protein kinase induces a p53-dependent metabolic checkpoint. Mol Cell 18:283–293

Kang J-H, Keller JJ, Chen C-S, Lin H-C (2012) Asian dust storm events are associated with an acute increase in pneumonia hospitalization. Ann Epidemiol 22:257–263

Kelly FJ, Fussell JC (2012) Size, source and chemical composition as determinants of toxicity attributable to ambient particulate matter. Atmos Environ 60:504–526

Khatri M, Bello D, Gaines P, Martin J, Pal AK, Gore R, Woskie S (2013) Nanoparticles from photocopiers induce oxidative stress and upper respiratory tract inflammation in healthy volunteers. Nanotoxicology 7: 1014–1027

Kumar P, Robins A, Vardoulakis S, Britter R (2010) A review of the characteristics of nanoparticles in the urban atmosphere and the prospects for developing regulatory controls. Atmos Environ 44: 5035–5052

Large DJ, Kelly S, Spiro B, Tian L, Shao L, Finkelman R, Zhang M, Somerfield C, Plint S, Ali Y (2009) Silica–volatile interaction and the geological cause of the Xuan Wei lung cancer epidemic. Environ Sci Technol 43:9016–9021

Leverson JD, H-k H, Forsburg SL, Hunter T (2002) The Schizosaccharomyces pombe aurora–related kinase Ark1 interacts with the inner centromere protein Pic1 and mediates chromosome segregation and cytokinesis. Mol Biol Cell 13:1132–1143

Li Q, Hu H, Jiang L, Zou Y, Duan J, SUN Z (2016): Cytotoxicity and autophagy dysfunction induced by different size of silica particles in human bronchial epithelial BEAS-2B cells. Toxicol Res

Li Y, Zhu T, Zhao J, Xu B (2012) Interactive enhancements of ascorbic acid and iron in hydroxyl radical generation in quinone redox cycling. Environ Sci Technol 46:10302–10309

Lim H, Bergvall C, Jarvis I, Mattsson Å, Dreij K, Stenius U, Westerholm R (2014) Benzo [a] pyrene-specific online high-performance liquid

chromatography fractionation of air particulate extracts–a tool for evaluating biological interactions. J Chromatogr A 1355:100–106

Lin H, Ning B, Li J, Ho SC, Huss A, Vermeulen R, Tian L (2015) Lung Cancer Mortality Among Women in Xuan Wei, China: A Comparison of Spatial Clustering Detection Methods. Asia Pac J Public Health 27(2):392–401

Lindeman TE, Poirier MC, Divi RL (2011) The resveratrol analogue, 2, 3′, 4, 5′-tetramethoxystilbene, does not inhibit CYP gene expression, enzyme activity and benzo [a] pyrene–DNA adduct formation in MCF-7 cells exposed to benzo [a] pyrene. Mutagenesis 26:629–635

Madl AK, Pinkerton KE (2009) Health effects of inhaled engineered and incidental nanoparticles. Crit Rev Toxicol 39:629–658

Matassoni L, Pratesi G, Centioli D, Cadoni F, Lucarelli F, Nava S, Malesani P (2011) Saharan dust contribution to PM 10, PM 2.5 and PM 1 in urban and suburban areas of Rome: a comparison between single-particle SEM-EDS analysis and whole-sample PIXE analysis. J Environ Monit 13:732–742

McClean M, Rinehart R, Ngo L, Eisen E, Kelsey K, Wiencke J, Herrick R (2004) Urinary 1-hydroxypyrene and polycyclic aromatic hydrocarbon exposure among asphalt paving workers. Ann Occup Hyg 48: 565–578

Melchini A, Catania S, Stancanelli R, Tommasini S, Costa C (2011) Interaction of a functionalized complex of the flavonoid hesperetin with the AhR pathway and CYP1A1 expression: involvement in its protective effects against benzo [a] pyrene-induced oxidative stress in human skin. Cell Biol Toxicol 27:371–379

Mendoza A, Torres-Hernandez JA, Ault JG, Pedersen-Lane JH, Gao D, Lawrence DA (2014) Silica nanoparticles induce oxidative stress and inflammation of human peripheral blood mononuclear cells. Cell Stress Chaperones 19:777–790

Møller P, Danielsen PH, Karottki DG, Jantzen K, Roursgaard M, Klingberg H, Jensen DM, Christophersen DV, Hemmingsen JG, Cao Y (2014) Oxidative stress and inflammation generated DNA damage by exposure to air pollution particles. Mutat Res/Rev Mutat Res 762:133–166

Nabeshi H, Yoshikawa T, Matsuyama K, Nakazato Y, Tochigi S, Kondoh S, Hirai T, Akase T, Nagano K, Abe Y (2011) Amorphous nanosilica induce endocytosis-dependent ROS generation and DNA damage in human keratinocytes. Part Fibre Toxicol 8:1

Napierska D, Thomassen LC, Lison D, Martens JA, Hoet PH (2010) The nanosilica hazard: another variable entity. Part Fibre Toxicol 7:1

Nemmar A, Albarwani S, Beegam S, Yuvaraju P, Yasin J, Attoub S, Ali BH (2014) Amorphous silica nanoparticles impair vascular homeostasis and induce systemic inflammation. Int J Nanomedicine 9: 2779

Nemmar A, Holme JA, Rosas I, Schwarze PE, Alfaro-Moreno E (2013): Recent advances in particulate matter and nanoparticle toxicology: a review of the in vivo and in vitro studies. BioMed Res Int 2013

Nemmar A, Yuvaraju P, Beegam S, Yasin J, Kazzam EE, Ali BH (2016) Oxidative stress, inflammation, and DNA damage in multiple organs of mice acutely exposed to amorphous silica nanoparticles. Int J Nanomedicine 11:919

Ouyang L, Shi Z, Zhao S, Wang FT, Zhou TT, Liu B, Bao JK (2012) Programmed cell death pathways in cancer: a review of apoptosis, autophagy and programmed necrosis. Cell Prolif 45:487–498

Pailler E, Auger N, Lindsay C, Vielh P, Islas-Morris-Hernandez A, Borget I, Ngo-Camus M, Planchard D, Soria J-C, Besse B (2015): High level of chromosomal instability in circulating tumor cells of ROS1-rearranged non-small-cell lung cancer. Ann Oncol, mdv165

Pink M, Verma N, Rettenmeier AW, Schmitz-Spanke S (2014) Integrated proteomic and metabolomic analysis to assess the effects of pure and benzo [a] pyrene-loaded carbon black particles on energy metabolism and motility in the human endothelial cell line EA. hy926. Arch Toxicol 88:913–934

Puente BN, Kimura W, Muralidhar SA, Moon J, Amatruda JF, Phelps KL, Grinsfelder D, Rothermel BA, Chen R, Garcia JA (2014) The oxygen-rich postnatal environment induces cardiomyocyte cell-cycle arrest through DNA damage response. Cell 157:565–579

Rieder CL (2011) Mitosis in vertebrates: the G2/M and M/a transitions and their associated checkpoints. Chromosom Res 19:291–306

Shi P, Chandra J, Sun X, Gergely M, Cortes JE, Garcia-Manero G, Arlinghaus RB, Lai R, Amin HM (2010) Inhibition of IGF-IR tyrosine kinase induces apoptosis and cell cycle arrest in imatinib-resistant chronic myeloid leukaemia cells. J Cell Mol Med 14: 1777–1792

Škarek M, Janošek J, Čupr P, Kohoutek J, Novotna-Rychetska A, Holoubek I (2007) Evaluation of genotoxic and non-genotoxic effects of organic air pollution using in vitro bioassays. Environ Int 33: 859–866

Sun L, Li Y, Liu X, Jin M, Zhang L, Du Z, Guo C, Huang P, Sun Z (2011) Cytotoxicity and mitochondrial damage caused by silica nanoparticles. Toxicol in Vitro 25:1619–1629

Tian L, Dai S, Wang J, Huang Y, Ho SC, Zhou Y, Lucas D, Koshland CP (2008) Nanoquartz in late Permian C1 coal and the high incidence of female lung cancer in the Pearl River origin area: a retrospective cohort study. BMC Public Health 8:1

Vakharia DD, Liu N, Pause R, Fasco M, Bessette E, Zhang Q-Y, Kaminsky LS (2001) Polycyclic aromatic hydrocarbon/metal mixtures: effect on PAH induction of CYP1A1 in human HEPG2 cells. Drug Metab Dispos 29:999–1006

Wang W, Li Y, Liu X, Jin M, Du H, Liu Y, Huang P, Zhou X, Yuan L, Sun Z (2013) Multinucleation and cell dysfunction induced by amorphous silica nanoparticles in an L-02 human hepatic cell line. Int J Nanomedicine 8:3533

Wannhoff A, Bölck B, Kübler A, Bloch W, Reuther T (2013) Oxidative and nitrosative stress and apoptosis in oral mucosa cells after ex vivo exposure to lead and benzo [a] pyrene. Toxicol in Vitro 27:915–921

WHO (2013) Health effects of particulate matter. Policy implications for countries in eastern Europe, Caucasus and Central Asia. World Health Organization Regional Office for Europe, Copenhagen

Yu Y, Duan J, Li Y, Yu Y, Jin M, Li C, Wang Y, Sun Z (2015) Combined toxicity of amorphous silica nanoparticles and methylmercury to human lung epithelial cells. Ecotoxicol Environ Saf 112:144–152

Zhu W, Cromie MM, Cai Q, Lv T, Singh K, Gao W (2014) Curcumin and vitamin E protect against adverse effects of benzo [a] pyrene in lung epithelial cells. PLoS One 9:e92992